Supporting Information

Lu et al. 10.1073/pnas.1219901110

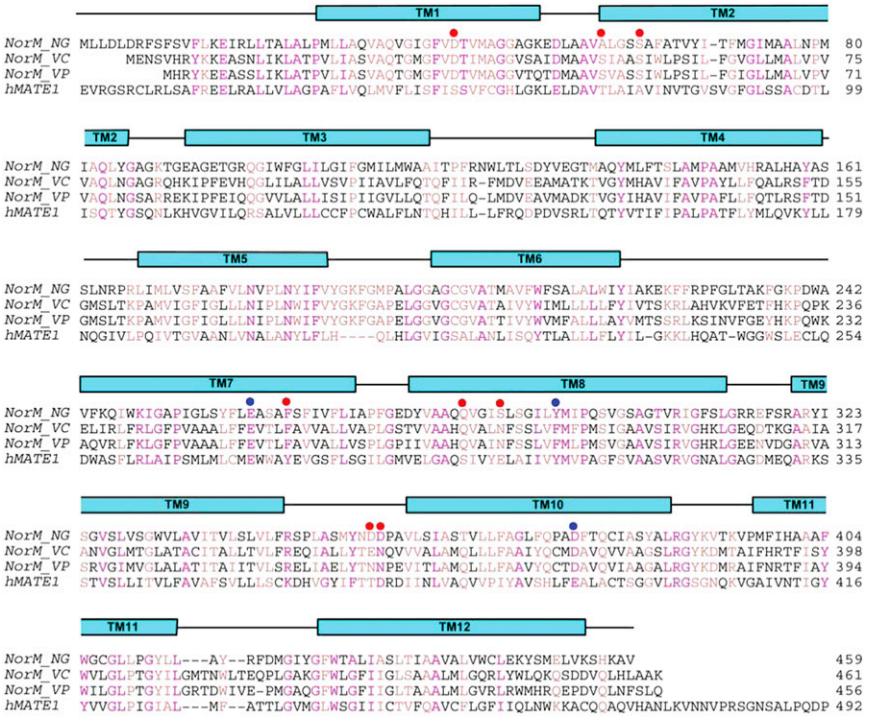

Fig. S1. Sequence alignment of Na^+-coupled multidrug and toxic compound extrusion (MATE) transporter (NorM)-NG with NorM-VC, NorM-VP, and hMATE1. Conserved and homologous residues are colored magenta and rose, respectively. Regions of transmembrane helices in NorM-NG are outlined according to dihedral angels (ϕ and ψ) and numbered. Blue and red dots indicate amino acids that coordinate Na^+ and interact with all three substrates, respectively. Residues 1–19 in hMATE1 are omitted for clarity.

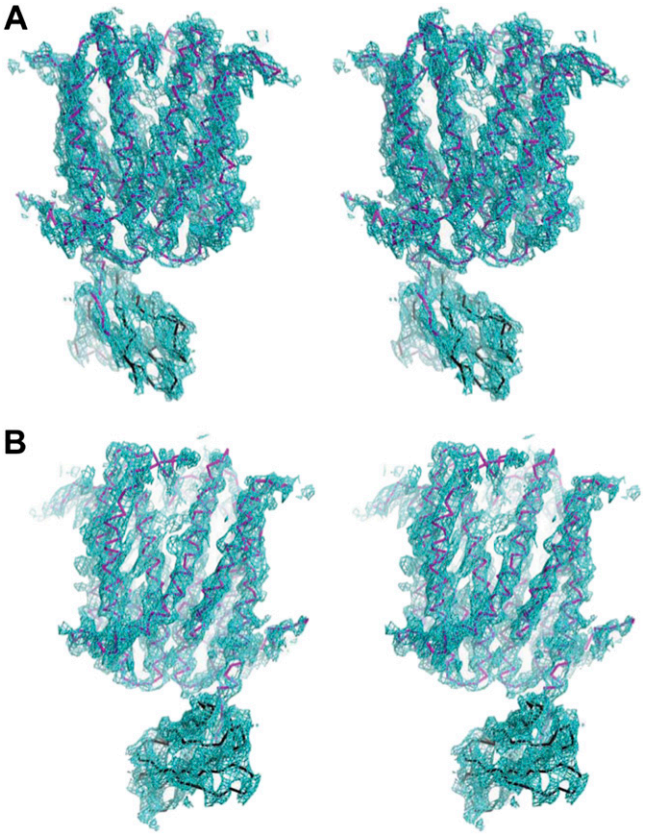

Fig. S2. Stereo views of the experimental electron density for the apo crystal form. The map was calculated to 3.5-Å resolution using density modified multiple isomorphous replacement and anomalous scattering (MIRAS) phases and contoured at 1.5 σ. Density modification included solvent flattening, histogram matching, cross-crystal averaging, and phase extension. The Cα backbone of NorM-NG is colored magenta, whereas that of monobody is in black. The view in *A* is related to that in *B* by an 180° rotation along the membrane normal.

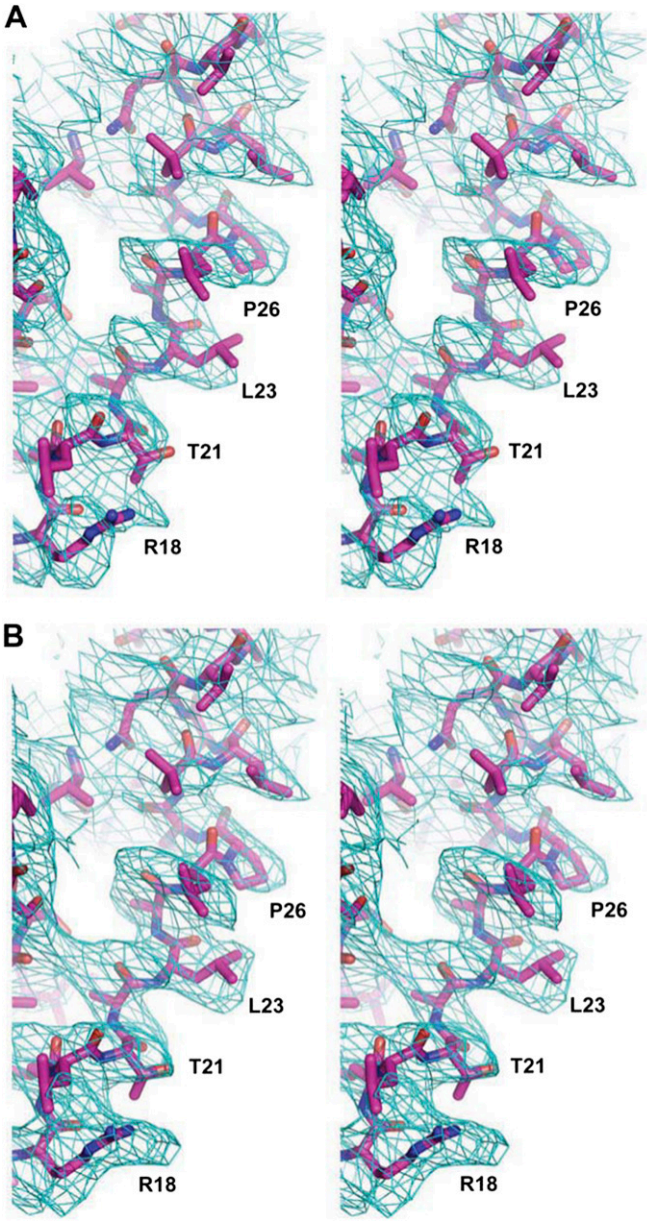

Fig. S3. Stereo views of representative electron density at 3.5-Å resolution for the apo crystal form. The featured slice depicts the amino end of TM1. Density modified MIRAS phases were used to calculate map shown in *A*, whereas the MIRAS phases were combined with model-derived phases before density modification to yield map in *B*. Both maps were contoured at 1σ.

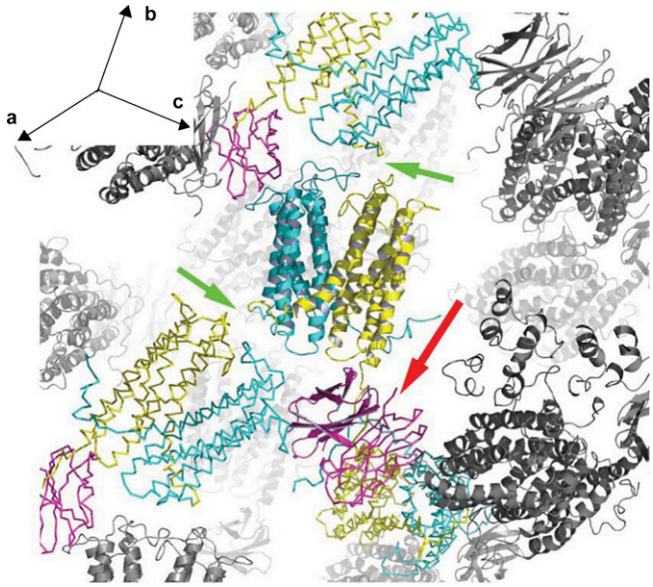

Fig. S4. Crystal packing in the apo crystal form. One complex of NorM-NG and monobody is drawn as ribbons, whereas its three neighboring complexes are displayed as backbone traces. NorM-NG is colored cyan (residues 5–230) and yellow (residues 231–459), whereas monobody is in magenta. Other molecules are shown as black ribbons. Red arrow highlights the extensive interactions mediated by monobody alone; green arrows indicate the packing interactions between adjacent NorM-NG molecules, which seem to stabilize the drug-bound conformation. *Inset* indicates the directions of unit cell axes.

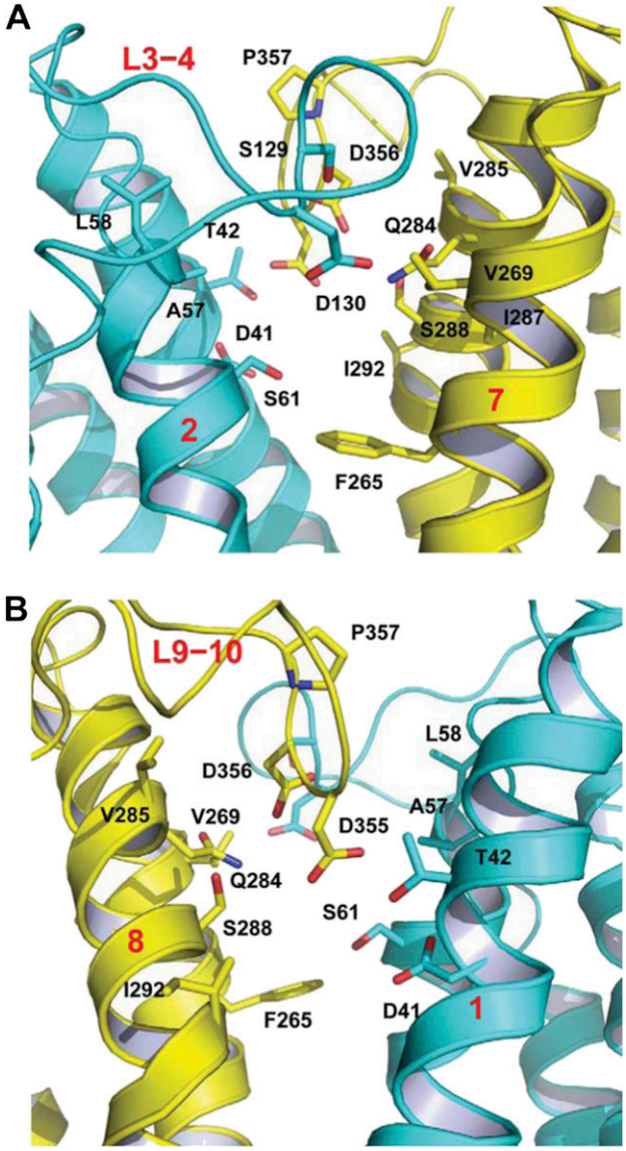

Fig. S5. Central cavity as viewed from the membrane plane. Views in *A* and *B* are related by a 180° rotation along the membrane normal. NorM-NG in ribbon rendition is colored cyan (residues 5–230) and yellow (residues 231–459). Amino acids within the cavity are drawn as stick models.

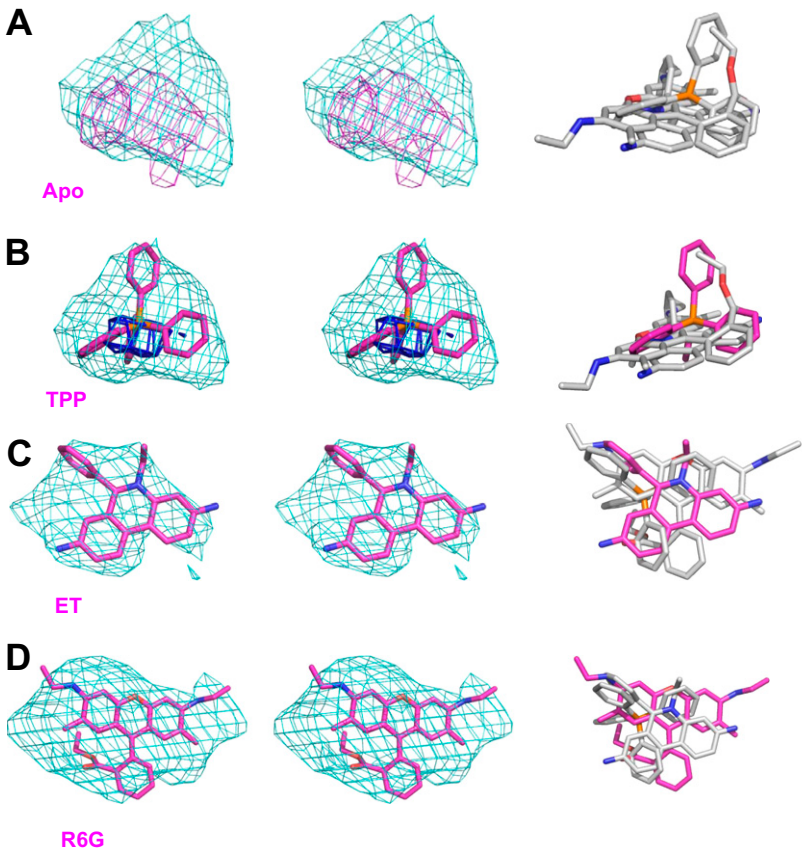

Fig. S6. Stereo views of the electron density for bound ligands. (*A*) The 3.5-Å-resolution Fo-Fc (Fo and Fc are the observed and calculated structure factors, respectively) map (magenta mesh) for the apo NorM-NG was overlaid onto that of the tetraphenylphosphonium (TPP)-bound form (cyan mesh), which was calculated to 3.6-Å resolution. Both maps were contoured at 3σ. (*B*) The Fo-Fc map at 3.6-Å resolution (cyan mesh) for the TPP-bound form (3σ) and a difference anomalous Fourier map (blue wire) from the arsonium analog of TPP (6.5 Å, 3.5σ) were overlaid onto the final model of TPP (magenta). (*C* and *D*) The 3.5- and 3.6-Å Fo-Fc maps (cyan mesh, 3σ) for the ethidium-bound and rhodamine 6G (R6G)-bound forms were overlaid onto the stick models (magenta) of ethidium (ET) and R6G, respectively. To minimize model bias, all of the phases were derived from protein models that had never been refined with the bound substrates. To orient the viewer, the refined models of three substrates were also superimposed onto each other, with the relevant drugs colored in magenta.

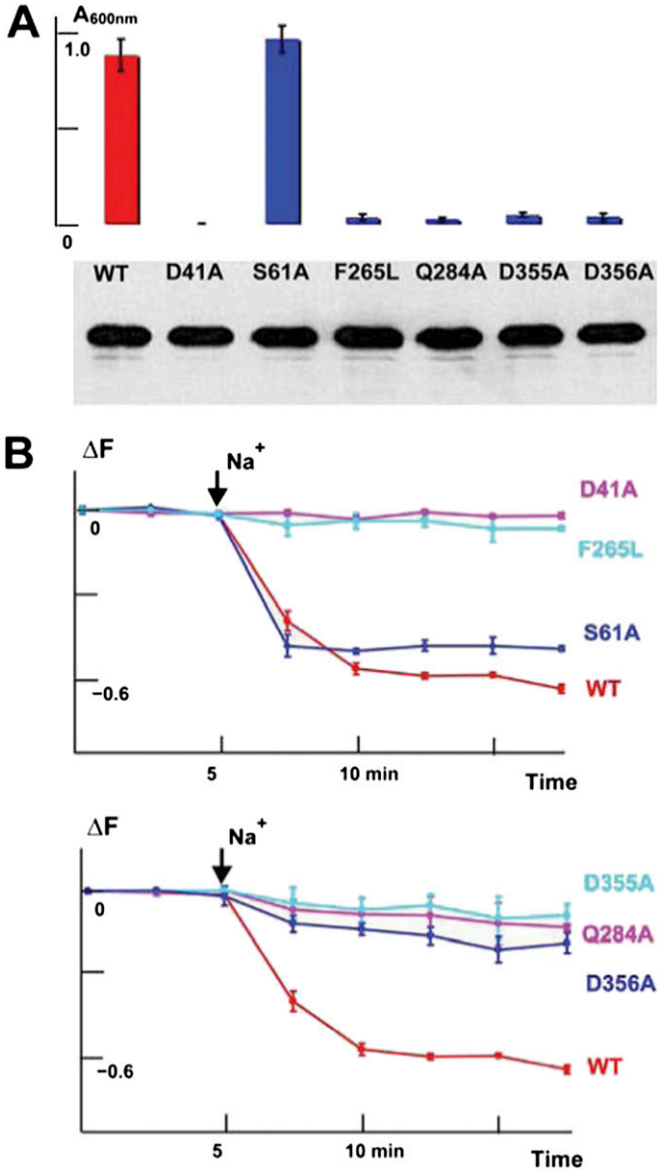

Fig. S7. Mutational effects on the substrate-binding site. (*A*) The inhibition of bacterial growth as measured by attenuance at 600 nm (A_{600nm}). Bacteria expressing the indicated NorM-NG mutants were grown in the presence of 3.0 μg/mL R6G. (*Inset*) Western blot analysis of NorM-NG mutants in membrane preparations. (*B*) Time course of fractional fluorescence reduction (ΔF) as a result of whole cell-based R6G efflux mediated by NorM-NG mutants. Reactions were started by the addition of 200 mM NaCl, as indicated by black arrows. In both *A* and *B*, error bars show SDs among three independent experiments (i.e., three different transformations) that were conducted in duplicate.

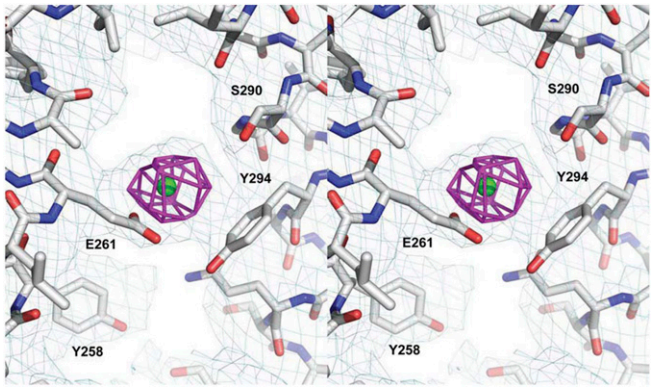

Fig. S8. Stereoview of the electron density for the Cs^+-binding site in NorM-NG. TM7 and TM8 are shown in stick representation, whereas Cs^+ is displayed as a green sphere. The 2Fo-Fc electron density map (light blue wire) was calculated to 3.8 Å and contoured at 1σ, whereas the difference isomorphous Fourier map (magenta mesh) was calculated to 6 Å and contoured at 6σ. Notably, the counterparts of E261 and Y258 in NorM-VC were among the nine amino acids that had been implicated in cation binding (1).

1. He X, et al. (2010) Structure of a cation-bound multidrug and toxic compound extrusion transporter. *Nature* 467(7318):991–994.

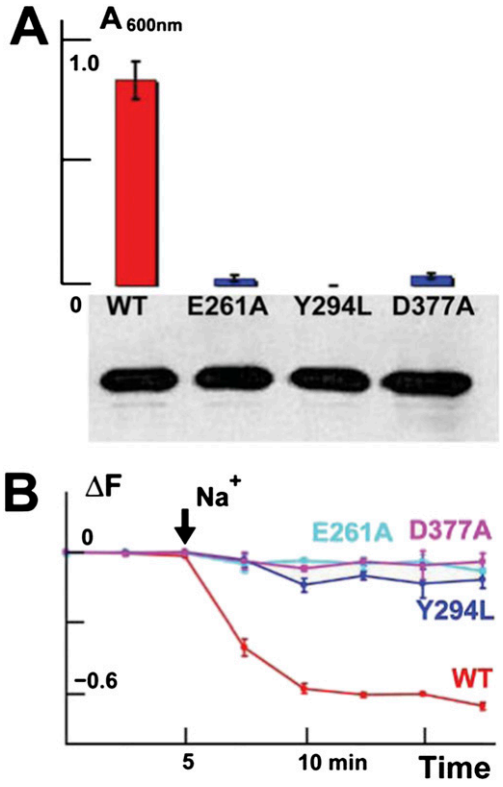

Fig. S9. Functional consequences of mutations in the cation-binding site. (*A*) The inhibition of bacterial growth as measured by attenuance at 600 nm (A_{600nm}). Bacteria expressing the indicated NorM-NG mutants were grown in the presence of 3.0 μg/mL R6G. (*Inset*) Western blot analysis of NorM-NG mutants in membrane preparations. (*B*) Time course of fractional fluorescence reduction (Δ*F*) as a result of whole cell-based R6G efflux mediated by NorM-NG mutants. Reactions were started by the addition of 200 mM NaCl, as indicated by black arrows. In both *A* and *B*, error bars show SDs among three independent experiments that were conducted in duplicate.

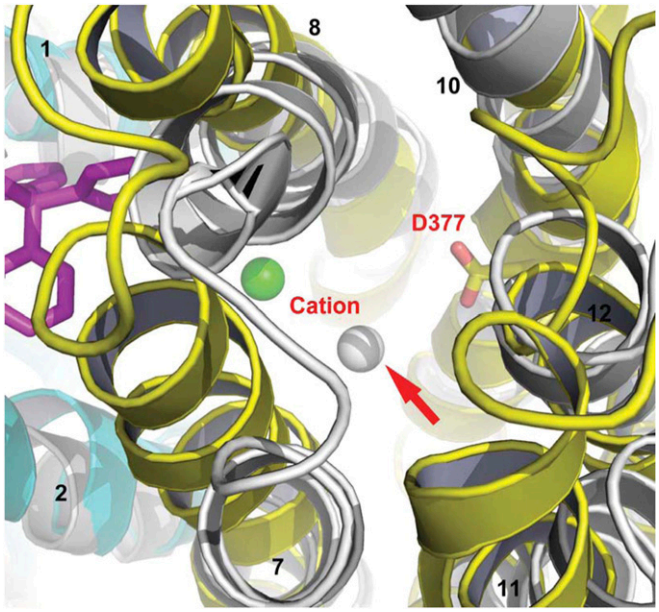

Fig. S10. Na^+ coordination in the substrate-free transporter likely involves D377. Cation-bound NorM-NG (cyan and yellow, PDB ID code 4HUL) and NorM-VC (gray, PDB ID code 3MKU) are shown as ribbon diagrams; TPP (magenta) and D377 in NorM-NG are drawn as stick models. TPP model was taken from the drug-bound structure (PDB ID code 4HUK) to indicate the substrate-binding site. Cations bound to NorM-NG and NorM-VC are depicted as green and gray sphere, respectively. Transmembrane helices are numbered. Structural superimposition of NorM-NG and NorM-VC placed the bound cation from NorM-VC (highlighted by a red arrow) in close proximity to D377, supporting the direct involvement of D377 in cation-coordination in the drug-free, Na^+-bound transporter (state 3 in Fig. 4).

Table S1. Data collection and phasing statistics for apo NorM-NG

	Native	EMTS	TMLA	TELA	K_2PtCl_4	$KAu(CN)_2$	TMLA + K_2PtCl_4	$KAu(CN)_2$ + K_2PtCl_4	CsCl
Wavelength (Å)	1.00	0.979	0.979	0.979	0.979	1.00	1.00	1.02	1.05
Space group	$P3_221$	$P3_221$	$P3_221$	$P3_221$	$P3_221$	$P3_221$	$P3_221$	$P3_221$	$P3_221$
a, *b*, *c* (Å)	118.21, 118.12, 226.59	119.13, 119.13, 226.61	117.75, 117.75, 227.18	117.67, 117.67, 227.20	118.68, 118.68, 228.76	117.98, 117.98, 226.84	118.45, 118.45, 227.96	119.40, 119.40, 228.04	118.3, 118.3, 227.32
Resolution (Å)	60–3.50	60–4.50	60–4.00	60–4.00	60–5.00	60–4.00	60–6.00	60–4.00	60–3.80
Observations	307,944	148,887	232,598	270,163	105,942	203,806	68,602	235,427	149,127
Unique reflections	23,025	11,540	15,977	15,891	10,846	15,692	4,984	16,221	18,316
Completeness (last shell)	98.6% (86.2%)	99.9% (100%)	99.9% (100%)	98.4% (88.5%)	94.8% (74.5%)	98.4% (95.3%)	98.9% (98.7%)	99.2% (99.5%)	98.3% (93.3%)
R_{sym} (last shell)*	11.0% (60.2%)	13.2% (58.7%)	10.7% (92.8%)	12.8% (98.7%)	12.2% (77.0%)	13.3% (94.0%)	8.4% (92.5%)	10.0% (76.3%)	11.8% (67.8%)
I/σ (last shell)	30.9 (1.5)	28.5 (2.5)	29.9 (2.2)	24.4 (1.0)	26.0 (0.8)	22.6 (1.3)	44.0 (2.1)	30.4 (1.9)	15.1 (1.3)
Phasing power (iso/ano)†	NA	1.28/0.61	2.00/0.72	1.82/NA	1.01/NA	1.79/NA	0.94/NA	0.93/NA	NA
R_{cullis} (iso/ano)‡	NA	0.69/0.98	0.50/0.98	0.58/NA	0.93/NA	0.55/NA	0.83/NA	0.63/NA	NA

Overall MIRAS figure of merit (defined as weighted mean value of the cosine of phase error; 20–4.0 Å): 0.69 (acentric), 0.72 (centric). EMTS, thimerosal; NA, not applicable; TELA, triethyllead acetate; TMLA, trimethyllead acetate.

*$R_{sym} = \Sigma|I - \langle I \rangle|/\Sigma I$, where I is the observed intensity of symmetry-related reflections.

†Phasing power = F_h/E, where F_h is the rms isomorphous/anomalous difference and E the rms residual lack of closure.

‡$R_{cullis}(iso) = \Sigma(||FPH - FP| - |FH(calc)||)/\Sigma(|FPH - FP|)$, where FPH and FP are structure factors for derivative and native data, respectively. R_{cullis}(iso) is valid for centric reflections only. $R_{cullis}(ano) = \Sigma(||\Delta FPH(obs)| - |\Delta FPH(calc)||)/\Sigma|\Delta FPH(obs)|$, where ΔFPH(obs) and ΔFPH(calc) are the observed and calculated structure factor differences between Bijvoet pairs, respectively.

Table S2. Data collection and phasing statistics for ethidium-bound NorM-NG

	Native	EMTS	TMLA	TELA	K_2PtCl_4
Wavelength (Å)	1.03	1.03	1.03	1.03	1.03
Space group	$P3_221$	$P3_221$	$P3_221$	$P3_221$	$P3_221$
a, *b*, *c* (Å)	119.03, 119.03, 227.48	116.41, 116.41, 224.99	117.66, 117.66, 226.29	117.91, 117.91, 226.88	116.94, 116.94, 227.97
Resolution (Å)	60–3.50	60–4.00	60–3.60	60–4.00	60–4.50
Observations	591,089	249,097	350,297	144,870	190,201
Unique reflections	24,111	15,190	21,803	16,104	10,979
Completeness (last shell)	98.9% (85.3%)	99.6% (100%)	99.1% (92.0%)	98.7% (96.3%)	99.2% (98.9%)
R_{sym} (last shell)*	11.0% (62.6%)	13.9% (74.7%)	13.1% (62.1%)	11.9% (62.9%)	11.7% (58.7%)
I/σ (last shell)	37.7 (1.5)	35.3 (2.9)	27.5 (1.7)	20.8 (1.7)	43.6 (3.1)
Phasing power (iso/ano)†	N.A.	1.17/0.49	1.23/0.45	1.13/0.47	1.01/0.44
R_{cullis} (iso/ano)‡	N.A.	0.76/0.96	0.78/0.97	0.81/0.99	0.81/0.96

Overall MIRAS figure of merit (defined as weighted mean value of the cosine of phase error; 20–3.60 Å): 0.37 (acentric), 0.45 (centric). EMTS, thimerosal; NA, not applicable; TELA, triethyllead acetate; TMLA, trimethyllead acetate.

*$R_{sym} = \Sigma|I - \langle I\rangle|/\Sigma I$, where I is the observed intensity of symmetry-related reflections.

†Phasing power = F_h/E, where F_h is the rms isomorphous/anomalous difference and E the rms residual lack of closure.

‡$R_{cullis}(iso) = \Sigma(||FPH - FP| - |FH(calc)||)/\Sigma(|FPH - FP|)$, where FPH and FP are structure factors for derivative and native data, respectively. R_{cullis}(iso) is valid for centric reflections only. $R_{cullis}(ano) = \Sigma(||\Delta FPH(obs)| - |\Delta FPH(calc)||)/\Sigma|\Delta FPH(obs)|$, where ΔFPH(obs) and ΔFPH(calc) are the observed and calculated structure factor differences between Bijvoet pairs, respectively.

Table S3. Data collection and phasing statistics for R6G-bound NorM-NG

	Native	EMTS	TMLA	TELA	K_2PtCl_4
Wavelength (Å)	1.03	1.03	0.939	0.939	1.03
Space group	$P3_221$	$P3_221$	$P3_221$	$P3_221$	$P3_221$
a, *b*, *c* (Å)	117.23, 117.23, 226.22	119.56, 119.56, 226.38	118.95, 118.95, 227.19	117.35, 117.35, 227.49	116.99, 116.99, 226.24
Resolution (Å)	60–3.60	60–4.00	60–4.00	60–4.00	60–5.00
Observations	503,078	177,389	272,323	227,942	82,064
Unique reflections	21,652	15,920	16,095	15,965	8,121
Completeness (last shell)	99.5% (99.7%)	98.9% (96.9%)	99.2% (99.7%)	99.5% (99.0%)	99.0% (100.0%)
R_{sym} (last shell)*	11.9% (68.4%)	12.6% (68.1%)	11.8% (71.3%)	12.8% (70.5%)	11.3% (63.2%)
I/σ (last shell)	36.0 (2.9)	31.6 (1.9)	31.4 (2.7)	22.6 (1.9)	40.5 (3.4)
Phasing power (iso/ano)†	NA	0.75/NA	1.22/0.46	1.26/0.47	1.08/0.38
R_{cullis} (iso/ano)‡	NA	0.93/NA	0.71/0.95	0.71/0.96	0.78/0.98

Overall MIRAS figure of merit (defined as weighted mean value of the cosine of phase error; 20–4.00 Å): 0.48 (acentric), 0.52 (centric). EMTS, thimerosal; NA, not applicable; TELA, triethyllead acetate; TMLA, trimethyllead acetate.

*$R_{sym} = \Sigma|I - \langle I\rangle|/\Sigma I$, where I is the observed intensity of symmetry-related reflections.

†Phasing power = F_h/E, where F_h is the rms isomorphous/anomalous difference and E the rms residual lack of closure.

‡$R_{cullis}(iso) = \Sigma(||FPH - FP| - |FH(calc)||)/\Sigma(|FPH - FP|)$, where FPH and FP are structure factors for derivative and native data, respectively. R_{cullis}(iso) is valid for centric reflections only. $R_{cullis}(ano) = \Sigma(||\Delta FPH(obs)| - |\Delta FPH(calc)||)/\Sigma|\Delta FPH(obs)|$, where ΔFPH(obs) and ΔFPH(calc) are the observed and calculated structure factor differences between Bijvoet pairs, respectively.

Table S4. Data collection and phasing statistics for TPP-bound NorM-NG

	Native	EMTS	TMLA	TELA	K_2PtCl_4	TPA
Wavelength (Å)	1.03	1.03	1.03	1.03	1.03	1.04
Space group	$P3_221$	$P3_221$	$P3_221$	$P3_221$	$P3_221$	$P3_221$
a, *b*, *c* (Å)	118.34, 118.34, 226.47	120.15, 120.15, 227.95	118.21, 118.21, 226.98	118.12, 118.12, 227.88	117.54, 117.54, 227.25	118.77, 118.77, 226.75
Resolution (Å)	60–3.60	60–3.60	60–3.80	60–4.00	60–4.50	60–4.50
Observations	795,483	274,600	221,897	110,497	53,845	161,718
Unique reflections	21,726	21,082	18,360	14,586	10,950	11,481
Completeness (last shell)	99.6% (100.0%)	98.5% (95.2%)	99.0% (98.6%)	92.3% (75.5%)	97.5% (91.4%)	99.6% (100.0%)
R_{sym} (last shell)*	10.7% (75.5%)	11.4% (67.1%)	12.8% (64.0%)	12.9% (57.1%)	11.2% (62.4%)	8.4% (70.7%)
I/σ (last shell)	59.3 (4.7)	36.2 (1.6)	28.5 (2.3)	20.0 (1.3)	17.1 (1.3)	38.7 (4.1)
Phasing power (iso/ano)†	NA	0.95/NA	1.30/NA	1.27/0.51	1.06/0.46	NA
R_{cullis} (iso/ano)‡	NA	0.89/NA	0.81/NA	0.82/0.98	0.83/0.98	NA

Overall MIRAS figure of merit (defined as weighted mean value of the cosine of phase error; 20–3.60 Å): 0.35 (acentric), 0.46 (centric). EMTS, thimerosal; NA, not applicable; TELA, triethyllead acetate; TMLA, trimethyllead acetate; TPA, tetraphenyl-arsonium (substrate analog).

*$R_{sym} = \Sigma|I - \langle I \rangle|/\Sigma I$, where I is the observed intensity of symmetry-related reflections.

†Phasing power = F_h/E, where F_h is the rms isomorphous/anomalous difference and E the rms residual lack of closure.

‡$R_{cullis}(iso) = \Sigma(||FPH - FP| - |FH(calc)||)/\Sigma(|FPH - FP|)$, where FPH and FP are structure factors for derivative and native data, respectively. $R_{cullis}(iso)$ is valid for centric reflections only. $R_{cullis}(ano) = \Sigma(||\Delta FPH(obs)| - |\Delta FPH(calc)||)/\Sigma|\Delta FPH(obs)|$, where ΔFPH(obs) and ΔFPH(calc) are the observed and calculated structure factor differences between Bijvoet pairs, respectively.

Table S5. Structure refinement statistics

	apo	ethidium	R6G	TPP	CsCl
Resolution (Å)	20.0–3.50	20–3.50	20–3.60	20–3.60	20–3.80
Number of reflections	21,935	22,889	20,561	20,600	17,371
R_{cryst}*	33.82%	31.41%	30.59%	30.68%	31.08%
R_{free}†	35.12%	33.13%	32.74%	34.94%	37.55%
Number of atoms	4,215	4,239	4,248	4,240	4,216
<B>	196.83	194.93	178.25	200.54	159.78
rms deviation					
Bond length (Å)	0.017	0.013	0.015	0.013	0.018
Bond angle	2.24°	2.13°	2.33°	2.15°	2.34°
Ramachandran					
Favored	94.1%	93.7%	92.3%	91.8%	93.0%
Allowed	5.9%	5.9%	6.6%	7.6%	5.9%
Disallowed	0%	0.4%	1.1%	0.6%	1.1%

*$R_{cryst} = \Sigma(||F_{obs}| - |F_{calc}||)/\Sigma(|F_{obs}|)$, where F_{obs} and F_{calc} are the observed and calculated structure factors, respectively.

†R_{free} is the same as R_{cryst} but calculated with 5% of the reflections excluded from structure refinement.

Table S6. Well-resolved NorM-NG residues and the basis of their assignment

Residue	Assignment basis
F8	Side chain density
F10	Side chain density
K15	Au binding
F39	Side chain density
M44	Pt binding
F63	Side chain density
Y67	Side chain density
F70	Side chain density
M71	Pt binding
M74	Pt binding
M80	Pt binding
Y85	Side chain density
K89	Au binding
F110	Side chain density
W116	Side chain density
W125	Side chain density
E133	Pb binding
H153	Au binding
H157	Au binding
Y159	Side chain density
M170	Pt binding
Y185	Side chain density
Y187	Side chain density
F192	Side chain density
C202	Hg/Pb binding
F210	Side chain density
W211	Side chain density
F212	Side chain density
W218	Side chain density
Y220	Side chain density
F226	Side chain density
F236	Side chain density
W241	Side chain density
W248	Side chain density
Y258	Side chain density
F259	Side chain density
E261	Pb binding
F265	Side chain density
Y294	Side chain density
F310	Side chain density
F317	Side chain density
W332	Side chain density
F345	Side chain density
Y353	Side chain density
D377	Pb binding
C381	Hg/Pb binding
K394	Au binding
H400	Au binding
C407	Hg/Pb binding
Y417	Side chain density
F419	Side chain density
C444	Hg/Pb/Au binding
Y448	Side chain density
M450	Pt binding
H456	Au binding
K457	Au binding

Table S7. MIC (μg/mL) of cells expressing NorM-NG variants

Drug	pET15b	WT	D41A	F265L	Q284A	D355A	D356A	S61A	E261A	Y294L	D377A
Ethidium	0.5	2.0	0.5	0.5	0.5	0.5	0.5	2.0	0.5	0.5	0.5
R6G	3.0	6.0	3.0	3.0	3.0	3.0	3.0	6.0	3.0	3.0	3.0
TPP	2.5	5.0	2.5	2.5	2.5	2.5	2.5	5.0	2.5	2.5	2.5

F265A, S288A, or Y294A completely abolished NorM-NG expression. The following drug concentrations were used: 0, 0.5, 1.0, 1.5, 2.0, 2.5, and 3.0 μg/mL ethidium; 0, 1.5, 3.0, 4.5, 6.0, 7.5, and 9.0 μg/mL R6G; and 0, 1.25, 2.5, 3.75, 5.0, 6.25, and 7.5 μg/mL TPP. MIC, minimal inhibitory concentration.